OPTO-ELECTRONICS REVIEW **13**(2), 157–169

Steady state photorefractive gratings in multiple quantum wells at high modulation depth

M. WICHTOWSKI*, E. WEINERT-RĄCZKA, and A. GAJDA

Institute of Electronics, Telecommunication and Informatics, Electrical Engineering Department, Szczecin University of Technology, 17 Piastów Ave., 70–310 Szczecin, Poland

The steady-state analytical expressions for the space-charge field harmonics generated by the high contrast interference pattern in biased photorefractive material with ambipolar transport are presented. As an example semi-insulating multiple quantum wells film operating in the Franz-Keldysh geometry was considered. Parameters of photorefractive grating created by a quadratic electro-optic effect were analysed. Calculations based on the band transport model were limited to the low external field case what corresponds to the linear transport regime. In particular, it was found that the photogenerated carriers density has nearly harmonic distribution. Moreover, the fundamental component can be obtained from the linear equations what enables us to improve the solution for the space-charge field in bulk, nonresonant materials described by the classical Kukhtarev's model

Keywords: photorefractive multiple quantum wells, band transport model, harmonic gratings.

1. Introduction

Dynamic holographic gratings in photorefractive (PR) materials are widely used in optical signal processing and materials characteristics measurements [1]. From theoretical point of view, PR effect is mostly described by the band transport model also called the PDDT (photogeneration-diffusion-drift-trapping) model [2] based on classical Kukhtarev's equations [3]. Photorefractive experiments as well as theoretical and numerical analyses are usually conducted for the sinusoidal light pattern. For the small modulation depth m, the PDDT equations can be linearized [4] and a solution limited to the first harmonic can be easily obtained [5,6]. In the case of materials with a linear electro-optic effect, this approximation corresponds to a linear response of the material and the superposition of multiple gratings is applicable. On the other hand, the stronger PR response is obtained for the high fringes contrast m. Hence, many experiments especially focused on applications, are carried out with $m \sim 1$. However, for the large modulation depth, strong departure from the harmonic distribution of the space charge appears and the exact analytic solution of the PDDT model does not exist. Thus, to solve this equation system for an arbitrary value of m numerical [7–12] and approximated methods [13–17] were developed. Almost all publications dedicated to this problem focus on the analysis of the Kukhtarev's model with a single type of charge carriers [7–17]. In one of the last publications [18], steady state solutions obtained within the electron-hole transport model were reported as exact solutions. However, the results are not consistent with the most of previous publications [13–17] and do not explain a dependence of the average electric current on the fringe contrast [17]. In fact, the perturbative method used in Ref. 18, like as in Refs. 19 and 20 fails for large value of m (see Ref. 21).

The simple unmodified Kukhtarev's model describing the most important features of photorefractive effect (PRE) in nonresonant, bulk materials is not adequate for several new, highly effective materials like PR polymers [22], PR liquid crystals [23] or PR multiple quantum wells (PR-MQW) [24,25].

In this paper, we deal with the PDDT model describing interband PRE [26] in semi-insulating semiconductor MQW's sample working with the dc external field parallel to the wells planes and to the light intensity changes [27]. Very high sensitivity and short response time (of the order of s) make PR-MQW material attractive for applications, especially in optical signal processing and real-time holography [25,27,28]. Free carriers in PR-MQW are mainly generated by interband transitions and photorefractive effect relies on the change of absorption caused by the influence of electric field on resonant exciton transitions in quantum wells. Changes in the index of the absorption and refraction (related by Kramers-Kronig formulas) depend on the squared electrical field intensity, in contrary to the classical linear electro-optic effect characteristic for non-resonant materials. The photorefractive properties of MQW films were investigated in GaAs-AlGaAs [25,27], ZnTe-CdZnTe [29], and GaAs-InGaAs [30] systems. In our calculations, we used parameters of the most common

*e-mail: marekw@ps.pl

GaAs-AlGaAs system. However, in this case two limitations should be taken into account. Firstly, for the fields of above 3–4 kV/cm, electrons mobility is reduced because of nonlinear transport caused by inter-valley scattering [31]. Moreover, the quadratic dependence of the absorption and refractive index changes on the electric field applies only for relatively small value of the electrical field (<10 kV/cm), with the value of limit depending on the quantum confinement strength in the considered structure [32]. Here, we restrict the analysis to the linear transport case, taking into account external electric fields below 3 kV/cm. However, it will be shown that for the high fringe contrast ($m \approx 1$) total electric field can locally be considerably higher than the external field what limits also the range of described modulation depths.

Nevertheless, in PR-MQW, in which photoconductivity is strongly dominated by holes transport, the effect of the velocity saturation caused by hot electrons appears at above 6–8 kV/cm [27]. In this case, the results presented here are valid even for the modulation depth in the range of 0.7–0.8.

2. Theoretical background

2.1. The band transport model

The simplest but commonly used PR transport model assumes two energy levels in the gap between valence and conduction band, one deep traps level (defects or impurities) and one shallow level of other species. Here, we assume that the deep donors N_D fully compensate the shallow acceptors ($N_A = N_A^- = \text{constant}$). When the non-uniform light pattern falls on the sample, free carriers excited in bright regions drift and diffuse and finally they are trapped in dark regions. As a consequence, the inhomogeneous space charge field forms and modulates the index of refraction through the electro-optic effect.

In Fig. 1, the most important PR transport processes are shown. In the case of conventional materials described by the one-band model, carriers are created by photoionization of defects and interband generation is omitted. In PR-MQW interband, absorption dominates and transitions 1', 1'' can be neglected. This difference significantly alters the PR properties of the materials.

We consider the material response under a stationary interference pattern

$$I(z) = I_0[1 + (m/2)\exp(iKz) + c.c.]g(z), \tag{1}$$

where $I_0 = I_1 + I_2$ is the average light intensity, $m = 2(I_1 I_2)^{1/2}/I_0$ is the modulation depth (fringes contrast), $K = 2\pi/\Lambda$, where Λ is the interference pattern period, and $g(z)$ describes the finite size of the light pattern. The sample is biased by a constant electric field applied in the z-direction, along quantum wells (so-called the Franz-Keldysh geometry). If we neglect the transverse carriers transport, the PDDT model can be reduced to the one-dimensional equations. The equations system, with the thermal generation

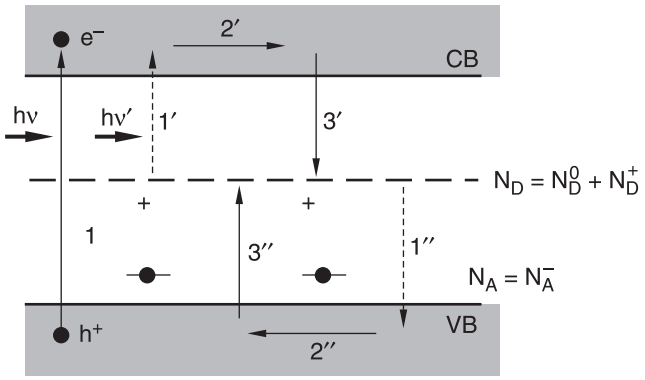

Fig. 1. Fundamental photorefractive transitions in the one-defect model. For PR-MQW the key role plays the inter-band absorption (transition 1), for the non-resonant materials the defects ionization (transitions 1' and 1'').

and the direct recombination of the carriers neglected, takes the following form [27,33]

$$\frac{\partial n_e}{\partial t} = (b + b_e)I - \gamma_e n_e N_D^+ + \frac{1}{q}\frac{\partial j_e}{\partial z}, \tag{2a}$$

$$\frac{\partial n_h}{\partial t} = (b + b_h)I - \gamma_h n_h N_D^0 - \frac{1}{q}\frac{\partial j_h}{\partial z}, \tag{2b}$$

$$\frac{\partial N_D^+}{\partial t} = (b_e - b_h)I + \gamma_h n_h N_D^0 - \gamma_e n_e N_D^+, \tag{2c}$$

$$j_e = q\mu_e n_e E_{tot} + \mu_e k_B T \frac{\partial n_e}{\partial z}, \tag{2d}$$

$$j_h = q\mu_h n_h E_{tot} - \mu_h k_B T \frac{\partial n_h}{\partial z}, \tag{2e}$$

$$\frac{\partial E_{tot}}{\partial z} = \frac{q}{\varepsilon_0 \varepsilon}(n_h + N_D^+ - n_e - N_A), \tag{2f}$$

where E_{tot} is the sum of the external field E_a and the space charge field E_{sc} ($E_{tot} = E_a + E_{sc}$).

The indices e and h refer to electrons and holes, respectively, n denotes the concentration of free carriers, N_D^+, N_D^0 are ionized and non-ionized donors ($N_D = N_D^0 + N_D^+$), N_A is the acceptors concentration, γ is the recombination coefficient, μ is the mobility of the carriers along the quantum wells. Term bI represents the inter-band free carriers generation rate, terms $b_e I$ and $b_h I$ the photo-generation from defects rates, where $b = \alpha/h\nu$, $b_e = s_e N_D^0/h\nu$ and $b_h = s_h N_D^+/h\nu$. Equation system (2a)–(2f) describes PR effect for resonant PR-MQW as well for non-resonant materials. In the first case, usually b_e, $b_h << b$ and in the second b_e, $i >> b$. Values of α, s_e, s_h, λ, and other parameters of GaAs wells used in calculations are listed in Table 1.

When the external dc electric field is applied, the equations system is supplemented by the boundary condition

$$\langle E_{tot} \rangle_L = E_a, \tag{2g}$$

where $\langle \ldots \rangle_L$ denotes spatial averaging over the grating length L.

Table 1. Parameters used in calculations.

Material parameters	
Cross section for photoionization of traps (Ref. 27)	$s_e = 1\times10^{-17}$ cm^2 $s_h = 1\times10^{-16}$ cm^2
Cross section for recombination to traps (Ref. 27)	$\sigma_e = 1\times10^{-14}$ cm^2 $\sigma_h = 5\times10^{-15}$ cm^2
Interband absorption coefficient (Ref. 27)	$\alpha = 10^4$ cm^{-1}
Trapping coefficient	$\gamma_e = 4\times10^{-7}$ cm^3/s $\gamma_h = 1\times10^{-7}$ cm^3/s
Carrier mobility (Ref. 33)	$\mu_e = 5000$ cm^2/Vs $\mu_h = 300$ cm^2/Vs
Compensation ratio of donors traps (Ref. 33)	$r = N_A/N_D = 0.5$
Writing wavelength (Ref. 33)	$\lambda_w = 630$ nm
Reading (resonant) wavelength (Ref. 27)	$\lambda = 835$ nm
Fringes contrast	$0 < m \le 1$
External electric field	$E_a \le 3$ kV/cm
Average light intensity	$I_0 = 10$ mW/cm^2

The trapping constants were estimated using the relation [34] $\gamma_i = \sigma_i v_{th(i)}$, $(i = e,h)$, where v_{th} is the average thermal velocity of the carriers.

$$V(z) = V_0 + \sum_{n=1}^{\infty} \tilde{V}_n \cos(nKz + \phi_n), \tag{4a}$$

where $V(z)$ describes the following variables n_e, n_h, N_D^+, j_e, j_h, and E_{sc}. The solutions include the amplitudes $\tilde{V}_n$ and the phase shifts ϕ_n of the Fourier components in respect to the interference pattern. Mathematically more convenient is the complex notation

$$V(z) \cong V_0 + \sum_{n=1}^{N} V_n \exp(inKz) + c.c. \tag{4b}$$

For the sake of calculations, the truncated Fourier expansions are used. Now, V_n indicates the complex amplitude of the n-th harmonic $V_n = |V_n|\exp(i\phi_n)$ where $|V_n| = \tilde{V}_n/2$.

Substituting Eq. (1) and Eq. (4b) to equations system (2a)–(2f) and comparing the components with the same $\exp(inKz)$ factor we get the algebraic equations system for the n-order harmonic amplitudes. For clarity, we have separated all expressions corresponding to the n-th harmonics and reduced the problem to three variables n_e, n_h, and N_D^+.

$$bI_0\left(\delta_{n,0} + \frac{m}{2}\delta_{n,1}\right) = n_{e(n)}\Gamma_{tote(n)} - n_{h(n)}\Gamma_{die}\bar{\delta}_{n,0} - N^+_{D(n)}(\Gamma_{die} - \Gamma_e)\bar{\delta}_{n,0} + \\ - \sum_{j=n-N}^{N}\left[\frac{n}{j}\Gamma_{die(n-j)}(N^+_{D(j)} + n_{h(j)} - n_{e(j)}) - \Gamma_{e(n-j)}N^+_{D(j)}\right]\bar{\delta}_{j,0}\bar{\delta}_{j,n}, \tag{5a}$$

$$bI_0\left(\delta_{n,0} + \frac{m}{2}\delta_{n,1}\right) = n_{h(n)}\Gamma_{toth(n)} - n_{e(n)}\Gamma_{dih}\bar{\delta}_{n,0} + N^+_{D(n)}(\Gamma_{dih} - \Gamma_h)\bar{\delta}_{n,0} + \\ - \sum_{j=n-N}^{N}\left[\frac{n}{j}\Gamma_{dih(n-j)}(N^+_{D(j)} + n_{h(j)} - n_{e(j)}) - \Gamma_{h(n-j)}N^+_{D(j)}\right]\bar{\delta}_{j,0}\bar{\delta}_{j,n}, \tag{5b}$$

$$0 = n_{h(n)}\Gamma_{Rh} - n_{e(n)}\Gamma_{\mathrm{Re}} - N^+_{D(n)}(\Gamma_e + \Gamma_h)\bar{\delta}_{n,0} - \sum_{j=n-N}^{N} N^+_{D(j)}(\Gamma_{e(n-j)} + \Gamma_{h(n-j)})\bar{\delta}_{j,0}\bar{\delta}_{j,n}, \tag{5c}$$

2.2. Harmonic amplitudes equations

We look for solutions of equations system (2a)–(2f) in the steady state. The period of the light pattern Λ is usually much smaller than the grating length what enables us to impose the periodic boundary conditions on $I(z)$, that is to take $g(z) \equiv 1$ in Eq. (1). In that case the condition of Eq. (2g) can be reduced to average over one grating period

$$\langle E_{sc} \rangle = 0. \tag{3}$$

Now, the solutions can be postulated in the periodic form [15,19]

where $\delta_{m,n}$ indicates the Kronecker delta function, and $\bar{\delta}_{m,n} = 1 - \delta_{m,n}$.

The n-th ($n \ge 1$) amplitude of the space charge field can be determined from the Gauss law, Eq. (2f)

$$E_n = \frac{q}{inK\varepsilon_0\varepsilon}(N^+_{D(n)} + n_{h(n)} - n_{e(n)}). \tag{5d}$$

The terms Γ_j expressing the processes rates per unit of time are listed in Table 2.

2.3. Zero order solutions

Zero order components depend on the average light intensity and can be derived from Eqs. (2a), (2b), and (2f) for homogenous illumination $I = I_0 =$ constant

Table 2. Electron and hole process rates.

Ion recombination rate	$\Gamma_{Re} = (\gamma_e N_D^+)^{-1}$	$\Gamma_{Rh} = (\gamma_h N_D^0)^{-1}$
Drift rate	$\Gamma_{Ee} = K\mu_e E_a$	$\Gamma_{Eh} = K\mu_h E_a$
Diffusion rate	$\Gamma_{De} = K_e E_d$	$\Gamma_{Dh} = K\mu_h E_d$
Dielectric relaxation rate	$\Gamma_{die} = q_e n_{e0}/\varepsilon_0\varepsilon$	$\Gamma_{dih} = q\mu_h n_{h0}/\varepsilon_0\varepsilon$
Carrier recombination rate	$\Gamma_e = {}_e n_{e0}$	$\Gamma_h = \gamma_h n_{h0}$
N-th order dielectric relaxation rate	$\Gamma_{die(n)} = q\mu_e n_{e(n)}/\varepsilon_0\varepsilon$	$\Gamma_{dih(n)} = q\mu_h n_{h(n)}/\varepsilon_0\varepsilon$
N-th order carrier recombination rate	$\Gamma_{e(n)} = \gamma_e n_{e(n)}$ $\Gamma_{tote(n)} = \Gamma_{\mathrm{Re}} + \Gamma_{die}\bar{\delta}_{n,0} + n^2\Gamma_{De} - in\Gamma_{Ee}$	$\Gamma_{h(n)} = \gamma_h n_{h(n)}$ $\Gamma_{toth(n)} = \Gamma_{Rh} + \Gamma_{dih}\bar{\delta}_{n,0} + n^2\Gamma_{Dh} + in\Gamma_{Ee}$

where $E_d = (k_B T/q)K$ is so-called diffusion field.

$$(N_{D0}^+)^3 - (N_D + N_A)(N_{D0}^+) + [N_D N_A - (\gamma_e^{-1} + \gamma_h^{-1})bI_0]N_{D0}^+ + bI_0\gamma_e^{-1}N_D = 0, \quad (6a)$$

$$n_{e0} = \frac{bI_0}{\gamma_e N_{D0}^+}, \qquad n_{h0} = \frac{bI_0}{\gamma_h(N_D - N_{D0}^+)}. \quad (6b, 6c)$$

To determine the higher harmonics we made two simplifying assumptions, the low light intensity $I_0 < 1$ W/cm^2 and sufficiently the large defects density $N_D > 10^{17}$ cm^{-3}. Both assumptions are fulfilled for the typical experimental conditions. In such a case, the free carriers densities are significantly smaller than the traps densities (n_e, $n_h \ll N_D^+$, N_D^0) and only slight traps depletion occurs [$\Delta N_D^+ \ll N_D^+(t=0) = N_A$ and $\Delta N_D^0 \ll N_D^0(t=0)$] what is called linear recombination approximation. In this case, the first order solution is $N_D^+ = N_A$, $n_{e0} = bI_0\tau_e$, and $n_{h0} = bI_0\tau_h$, where $\tau_{e,h}$ are the average lifetimes of electrons and holes

$$\tau_e = (\gamma_e N_A)^{-1}, \qquad \tau_h = [\gamma_h(N_D - N_A)]^{-1}. \quad (6d, 6e)$$

In the result of the above assumptions, the carrier density and dielectric relaxation rate products in equation system (5a)–(5c) can be neglected and in Eq. (5d) we have $E_{(n)} \sim N_{D(n)}^+$.

3. Dependence of the harmonic on lower order components

3.1. Non-coupled equations

In a general case, equation system (5a–5c) has only numerical solutions, because each harmonic is coupled with the higher order harmonics as well as with the lower order ones. Disregarding influence of the higher order harmonics ($\nu > n$) on the n-th components corresponds to a perturbative approach, where $\Delta I(z) = mI_0\cos(Kz)$ is treated as a perturbation of homogenous illumination and the modulation depth m as the perturbation parameter. That kind of procedure is correct when $m^3 \ll m$ (practically up to $m \leq 0.8$), but fails when m tends to unity. However, in this approximation the contribution from the most important harmonics is taken into account, thus this kind of solution is a good starting point to the solution of the complete equation system (5a–5c). Further, for simplicity, full equation system (5a–5c) will be called the coupled equations while equations with a neglected influence of the higher order components – the non-coupled equations. So, taking only the components from $j = 1$ to $n - 1$ we get the linear non-coupled equations system in the form

$$\boldsymbol{W}_n\boldsymbol{V}_n = \boldsymbol{F}_n, \quad (7)$$

where

$\boldsymbol{V}_n = [n_{e(n)}\ n_{h(n)}\ N_{D(n)}^+]^T$ is the vector of variables,

$$\boldsymbol{W}_n = \begin{bmatrix} \Gamma_{Re} - in\Gamma_{Ee} + n^2\Gamma_{De} & 0 & (-\Gamma_{die} + \Gamma_e)\bar{\delta}_{n,0} \\ 0 & \Gamma_{Rh} - in\Gamma_{Eh} + n^2\Gamma_{Dh} & (\Gamma_{dih} - \Gamma_h)\bar{\delta}_{n,0} \\ -\Gamma_{Re} & \Gamma_{Rh} & (-\Gamma_e - \Gamma_h)\bar{\delta}_{n,0} \end{bmatrix} \quad (7a)$$

is the matrix of process rates, and $\boldsymbol{F}_n$ is the "excitation" vector

$$\boldsymbol{F}_n = \begin{bmatrix} bI_0\left(\delta_{n,0} + \frac{m}{2}\delta_{n,1}\right) + \sum_{j=1}^{n-1}\left(\frac{n}{j}\Gamma_{die(n-j)} - \Gamma_{e(n-j)}\right)N_{D(j)}^+ \\ bI_0\left(\delta_{n,0} + \frac{m}{2}\delta_{n,1}\right) - \sum_{j=1}^{n-1}\left(\frac{n}{j}\Gamma_{dih(n-j)} - \Gamma_{h(n-j)}\right)N_{D(j)}^+ \\ \sum_{j=1}^{n-1}\left(\Gamma_{e(n-j)} + \Gamma_{h(n-j)}\right)N_{D(j)}^+ \end{bmatrix} \quad (7b)$$

The space charge field E_{sc} harmonics can be obtained from Eq. (5d) neglecting $n_{e(n)}$ and $n_{h(n)}$. For $n = 1$ one gets the linear solution.

3.2. Harmonics of the carriers densities and space charge field

The numerical solution of Eq. (7) shows, that for arbitrary set of the values of Λ, N_D, m, and E_a the first harmonic strongly dominates in the free-carriers spectra. The phase shift of the first harmonics in respect to the light intensity distribution is close to zero. Similar result was obtained numerically for the one-band Kukhtarev's model in Refs. 11,17. The dependence of $|n_{e(2)}|/|n_{e(1)}|$ ratio, (expressing the contribution of the higher harmonics), on E_a and the effective traps density $N_{eff} = r(1 - r)N_D$, for $m = 1$ is shown in Fig. 2.

It should be noticed that the plots were calculated numerically from the complete set of equations, without linear recombination approximation. From Fig. 2, we can infer that for the high traps concentration, the contribution of higher harmonics to $n_{e,h}(z)$ can be neglected. However, when N_{eff} is small and E_a is large, the $n_{e,h}(z)$ distribution can significantly depart from sinusoidal shape what is shown in Fig. 3. This conclusion is different from the result in Refs. 11 and 17, where the higher harmonics contribution was neglected in every case.

Then for typical, high N_{eff}, the electron and hole distribution can be expressed as

$$\begin{aligned}\tilde{n}_{e,h}(z) &= n_{e,h0} + \tilde{n}_{e,h1}(z) \\ &= n_{e,h0}[1 + m_{1e,h}\cos(Kz + \phi_{e,h})]\end{aligned}, \tag{8}$$

where $\phi_{e,h}$ 0 and $m_{1e} \approx m_{1h} = m_1$. Difference between ϕ_e and ϕ_h occurs only for strong diffusion currents ($\Lambda < 1$ μm). On the basis of linear equations [Eq. (7) for $n = 1$] we find that the carrier density modulation depth is given by

$$m_1(K) = \frac{m}{1 + K^2 L_D^2 \zeta}, \tag{8a}$$

where

$$L_D^2 = 2\frac{k_B T}{q}\left(\frac{1}{\mu_h \tau_h} + \frac{1}{\mu_e \tau_e}\right)^{-1}$$

is bipolar diffusion length [27,35], (8b)

$$\zeta = 1 + \frac{E_a^2 + E_d^2}{2E_q E_d}, \tag{8c}$$

$$E_q = qN_{eff}/(\varepsilon\varepsilon_0 K) \tag{8d}$$

is the saturation field [34].

Note incidentally, that describing the electron and hole gratings by the same expression involves automatically the small trap depletion. This conclusion is immediately apparent from Eq. (2c). In fact, assuming $n_{e,h}(z) = n_{e,h0}[1 + p(z)]$, where $p(z)$ is arbitrary periodic function and inserting this expressions to Eq. (2c) one gets

$$N_D^+(z) \approx \frac{\gamma_h n_{h0} N_D}{\gamma_h n_{h0} + \gamma_e n_{e0}} = N_{D0}^+ = \left\langle N_D^+(z) \right\rangle.$$

The ionized donors distribution is approximately equal to the average value. It means, that significant modulation depth of $N_D^+(z)$ is obtained provided that free carrier distributions n_e and n_h are different.

Neglecting of $n_{e,h(n)}$ components for $n > 1$ allows us to express the vector $\mathbf{F}_n$ in the simplified form

$$\boldsymbol{F_n} = \begin{bmatrix} \dfrac{n}{n-1}\Gamma_{die(1)} N_{D(1)}^+ \\ \dfrac{-n}{n-1}\Gamma_{dih(1)} N_{D(1)}^+ \\ (\Gamma_{e(1)} + \Gamma_{h(1)}) N_{D(1)}^+ \end{bmatrix} \tag{9}$$

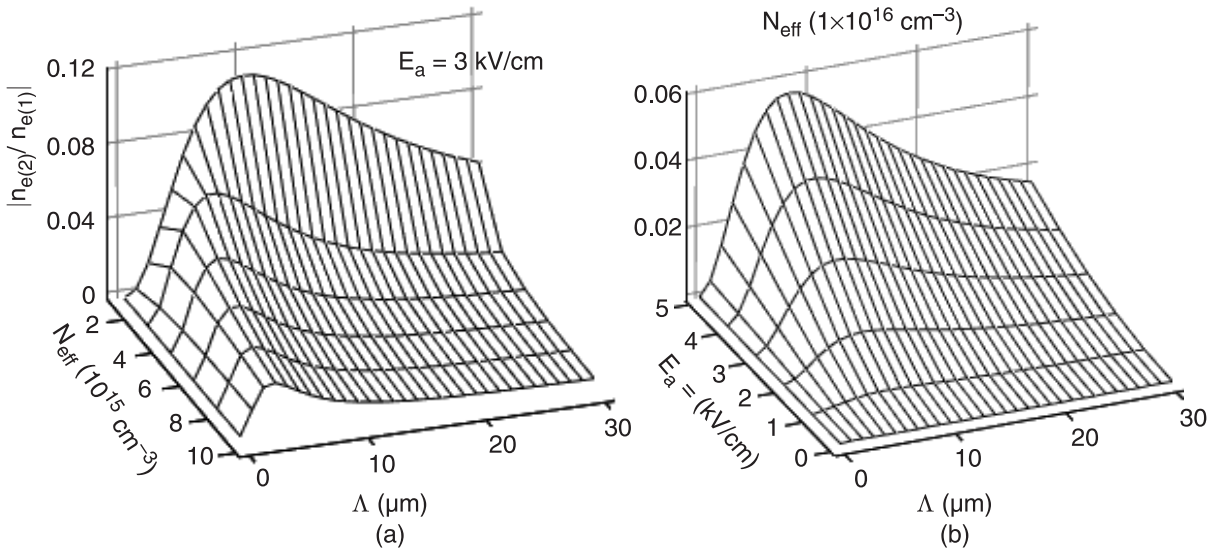

Fig. 2. Amplitude of the second harmonic of electron density against the first one as a function of the grating period and the effective trap concentration (a), the applied electric field (b), obtained from numerical solution of Eq. (7). High modulation depth, $m = 1$, is assumed.

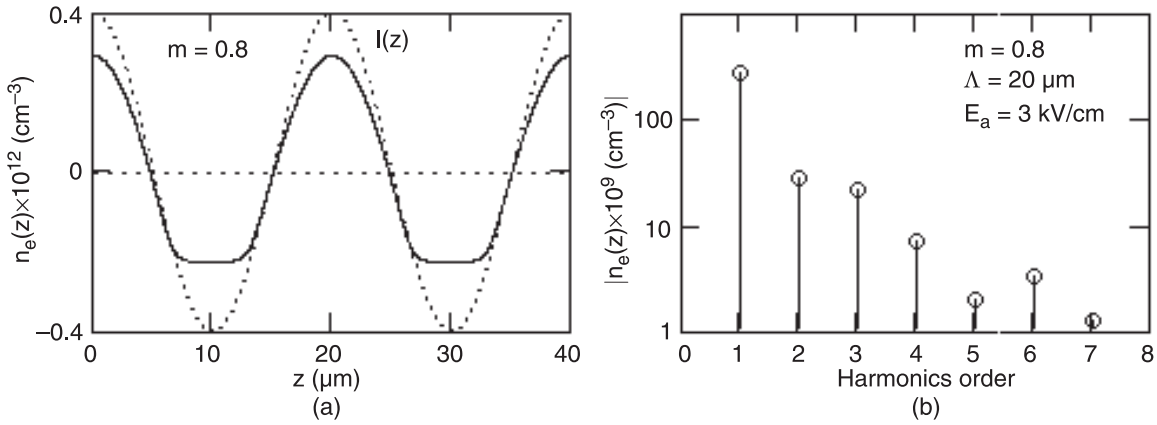

Rys. 3. The electrons density distribution (solid line) for the effective traps concentration of 2×10^{15} cm^{-3} and an external electric field of 3 kV/cm (a). The dotted line denotes the light intensity distribution. Harmonics amplitudes spectrum for the electrons density distribution (b).

where the terms $\Gamma_{e(n)}$, $\Gamma_{h(n)}$ were disregarded because for the material parameters characteristic for MQW (Table 1) holds $\Gamma_{e(n)}$, $\Gamma_{h(n)} << \Gamma_{die(n)}$, $\Gamma_{dih(n)}$. Note, that this relation arises from material parameters, hence for the considered material system is always satisfied. Substituting vector of Eq. (9) to Eq. (7) and using the Cramer's law one can find the expression for the complex amplitude of the n-th harmonics of $E_{sc}(n \geq 1)$

$$\tilde{E}_n = 2h^n(m_1)(E_a + i\xi E_d), \tag{10a}$$

$$h(m_1) = -\frac{m_1}{2}, \tag{10b}$$

$$\xi = \frac{\mu_e\tau_e - \mu_h\tau_h}{\mu_e\tau_e + \mu_h\tau_h}, \tag{10c}$$

where $\xi = \xi(N_D,r,\mu_{e,h},\gamma_{e,h})$ is so-called competition factor between electrons and holes, ranging from –1 to 1.

For $n = 1$, Eq. (10.1) is convergent to the formula derived in Ref. 33 and it is equal to the formula in Refs. 27 and 35 if $\zeta = 1$ is set in Eq. (8a). Both mentioned solutions are expressed in terms of the characteristic electric fields.

4. Influence of higher order harmonics

The formula describing the field profile $E_{sc}(z)$ for arbitrary value of m can be derived from currents densities of Eqs. (2d) and (2e) for the carriers density distribution analogous to Eq. (8)

$$\hat{n}_{e,h}(z) = n_{e,h0} + \hat{n}_{e,h1}(z) = n_{e,h0}[1 + a_1\cos(Kz)], \tag{11}$$

where $\hat{n}_{e,h}(z)$ is the carriers distribution in the case of coupling with higher harmonics included, and a_1 is an unknown modulation depth coefficient. We expect that for small modulation depth $a_1 \approx m_1$. The symbol ^ marks that the coupled amplitudes are used. In this case the sum of Eqs. (2d) and (2e) gives

$$J_0 = j_e(z) + j_h(z) = \sigma[1 + a_1\cos(Kz)][E_a + E_{sc}(z)], \tag{12}$$
$$+ a_1E_d\sin(Kz)(\sigma_h - \sigma_e)$$

where $J_0 = \langle J_0 \rangle$ = constant according to the continuity equation in the stationary state and the following designations were introduced: $\sigma_h = q\mu_h n_{h0}$, $\sigma_e = q\mu_e n_{e0}$, and the total conductivity $\sigma = \sigma_e + \sigma_h$.

Determining $E_{sc}(z)$ from Eq. (12) and using the boundary condition of Eq. (3) we get

$$J_0 = \sigma E_a\left\langle\frac{1}{1 + a_1\cos(Kz)}\right\rangle = \sigma E_a\sqrt{1 - a_1^2} \tag{13}$$

Substituting Eq. (13) to Eq. (12) and noting that $\xi = (\sigma_e - \sigma_h)/\sigma$ yields $E_{sc}(z)$ as

$$E_{sc}(z) = \frac{E_a\sqrt{1 - a_1^2} + a_1\xi E_d\sin(Kz)}{1 + a_1\cos(Kz)} - E_a. \tag{14}$$

Calculating the Fourier transform of Eq. (14) one finds

$$\tilde{E}_n = 2f^n(a_1)(E_a + i\xi E_d). \tag{15a}$$

$$f(a_1) = \frac{\sqrt{1 - a_1^2} - 1}{a_1} \tag{15b}$$

For the small m, when $a_1 \approx m_1$, the functions $f(a_1)$ and $h(m_1)$ are very similar, $f(a_1) \approx h(m_1)$.

The Poisson's equation gives the expression describing distribution of the ionized donors

$$N_D^+(z) = a_1\frac{\varepsilon_0\varepsilon K}{q} \times\frac{E_a\sqrt{1 - a_1^2}\sin(Kz) + \xi E_d(a_1 + \cos(Kz))}{(1 + a_1\cos(Kz))^2} + N_A \tag{16}$$

Equation (15b) can be obtained from coupled system of equations (5a)–(5c) only under the condition that $a_1 = m_1$. For that purpose one can consider one from equations for $n = 1$, for example Eq. (5a). Taking advantage of Eq. (5d)

and Eq. (10.1) we introduce the notation $N^+_{D(n)} = nh^nA$ and $\hat{N}^+_{D(n)} = nf^nA$, where $A = (iK\varepsilon_0\varepsilon/q)(E_a + i\xi E_d)$, and $f(a_1)$ is an unknown function replacing the function $h(m_1)$ for the large m. Setting $\hat{n}_{e(1)} = n_{e(1)}$, what corresponds to $a_1 = m_1$, in Eq. (5a) gives the coupled amplitude $\hat{N}^+_{D(1)}$ as a sum of the uncoupled amplitude $N^+_{D(1)}$ and the correction term $C_{HH(1)}$ arising from coupling with higher harmonics

$$\hat{N}^+_{D(1)} = N^+_{D(1)} + C_{HH(1)}, \tag{17}$$

where

$$\begin{aligned} N^+_{D(1)} &= \Gamma^{-1}_{die}\left(n_{e(1)}\Gamma_{tote(1)} - \frac{m}{2} bI_0 \right), \\ C_{HH(1)} &= -\Gamma^{-1}_{die} \sum_{j=1-N}^{N} j^{-1}\Gamma_{die(1-j)}\hat{N}^+_{D(j)}\bar{\delta}_{j,0}\bar{\delta}_{j,1} \end{aligned} \quad . \tag{18}$$

The terms $\Gamma_{e(1\text{-}j)}$ and $n_{e(j)}$, $n_{h(j)}$ were dropped according to the previous estimations, sec. (3.2).

Because $|n_{e(1)}| >> |n_{e(n)}|$ for $n > 1$, the $C_{HH(1)}$ can be reduced to the form

$$C_{HH1} \approx -\frac{n_{e(-1)}}{2n_{e0}}\hat{N}^+_{D(2)} = \left(-\frac{m_1^*}{4} \right) 2f^2A, \tag{19}$$

but $m_1^* = m_1$ because m_1 is the real quantity [see Eq. (8a)] and Eq. (17) can be written as

$$fA = (-m_1/2)A + (-m_1/2)f^2A, \tag{20}$$

leading to Eq. (15b). In the same manner, the function $f(a_1)$ can be derived from coupled equations for $n > 1$, providing that $a_1 = m_1$ what suggests the general assumption $\hat{n}_{e(n)} = n_{e(n)}$ for the arbitrary order n. Indeed, application of the amplitudes $\hat{N}^+_{D(n)} = f^n(m_1)N^+_{D(n)}$ and $\hat{n}_{e(n)} = n_{e(n)}$ in a system of equations (5a)–(5c) leads to very good convergence of equations. Then, taking into account the influence of coupling with higher harmonics is equivalent to multiplication of the space-charge amplitudes by $f^n(m_1)$, whereas the amplitudes of carrier densities stay unchanged what is in our opinion one of the most important results of this paper.

5. Harmonics in PR-MQW and in conventional materials

Within the framework of the classical one-band transport model described by a system of equations (2a)–(2f) with $V_h = 0$ and $b = 0$, many authors [1,15–17] obtained a formula for the space charge field E_{sc} components similar to Eq. (15a); (for one kind of carriers $|\xi| = 1$ is put). The most important difference is that instead of the carrier grating modulation depth $m_1(\Lambda)$ the light modulation depth m appears. The solution in the form

$$\tilde{E}_n = 2f^n(m)(E_a + iE_d); \quad f(m) = \frac{\sqrt{1-m^2}-1}{m}; \tag{21}$$

is usually called the Moharam's solution [1,37]. The relationship $m_1 = m$ comes from the fact, that (besides of the assumptions as in sec. 2.2) usually $N^+_D << N_D$is assumed, hence $N_D - N^+_D \cong N_D$ is substituted. If this approximation is discarded, the fundamental harmonic obtained from the linearized material equations [1,3,5] has the form

$$\tilde{E}_1 = \frac{-m}{1 + K^2L^2_{Db} - i\dfrac{E_a}{E_q}}(E_a + iE_d), \tag{22}$$

where $K^2L^2_{Db} = E_d/E_q$, *and* L_{Db} is the Debye's screening length.

Equation (22) is called the Kukhtarev's solution. It should be noted that for $m << 1$ and $E_q >> E_a$, E_d, Eq. (21) tends to Eq. (22). It means, that the Mohram's solution does not take into account saturation of the space charge field, what is possible for the limited traps density. Both solutions predict different results for $\Lambda \to 0$. Equation (21) gives $E_n \to \infty$, while Eq. (22) gives $E_n \to 0$. Moreover, the Moharam's formula leads to some complications for $m = 1$ [9].

The difference between the solutions can be eliminated using the similar way as in sec. 4. From the linear solution for $n = 1$, the free electrons grating modulation coefficient is

$$m_1 = \frac{\tilde{n}_{e(1)}}{n_{e0}} = \frac{m}{1 + K^2L^2_{Db} - i\dfrac{E_a}{E_q}} = |m_1|e^{i\phi}. \tag{22a}$$

Derivation like in sec. 4 leads to the Fourier transforms of the field E_{sc}

$$\tilde{E}_n = 2f^n(|m_1|)e^{in\phi}(E_a + iE_d). \tag{22b}$$

For the small value of m, the amplitude $\tilde{E}_1$ from Eq. (18b) is given by the same expression as $\tilde{E}_1$ from (22). Comparing Eq. (22b) and Eq. (15a) one sees, that the fundamental difference is that for PR-MQW the coefficient m_1 and amplitudes $\tilde{E}_n$, depend on the bipolar diffusion length L_D, while for the non-resonant materials they depend on the Debye's screening length L_{Db}.

6. Linear and nonlinear material response range

In general, deviation of the donors density $N^+_D(z)$ and the space charge field $E_{sc}(z)$ from the sinusoidal distributions depends on the light intensity modulation depth m, the fringe spacing Λ, the traps concentration N_{eff}, and the magnitude of the applied external field E_a [19]. The assumption

of linear recombination gives $n_{e,h0} \sim I_0$. In this case, starting from Eq. (7) and using the induction principle one can find that all amplitudes $n_{e,h(\nu)}$ are proportional to I_0 and $N^+_{D(\nu)}$ do not depend on I_0 for any ν. Likewise it can be shown, that $[n_{e(\nu)}, n_{e(\nu)}, N^+_D]^T \sim m^\nu$, from where using Eq. (5d) one obtains

$$\tilde{E}_{(\nu)} \sim m^\nu. \tag{23}$$

that stays in agreement with Eq. (10a) and perturbations calculations procedure. Therefore it is not a surprise that identical formula was established in Refs. 18, 19, and 20.

In order to show how the space charge field deviation from harmonic distribution (often called a nonlinearity) varies with the grating period, the dependence of $E_{(n)}$ on Λ for the biased and unbiased sample is presented in Fig. 4. In the case of $E_a = 0$, every curve has the maximum. For the amplitude $n = 1$ this maximum appears for the light pattern period close to

$$\Lambda_B = 2\pi L_D. \tag{24}$$

This result differs from the solution of Eq. (18), where $\Lambda_B = 2\pi L_{Db}$ [18,19]. On the basis of the plots from Fig. 4 the characteristic period Λ_B can be treated as the border between the linear and nonlinear response ranges. For $\Lambda << \Lambda_B$, the amplitudes of the higher harmonics are much smaller than the fundamental one, regardless of the modulation depth m. Likewise the fundamental harmonic dominates for $\Lambda >> \Lambda_B$ and $m << 1$. Both cases represent the linear response. For $\Lambda >> \Lambda_B$ and $m \sim 1$ higher harmonics become important and the response is strongly nonlinear. The dependence of $S_n = \left|\tilde{E}_n\right| / \left|\tilde{E}_1\right|$ for $n = 2$, 3, and 4, on the grating period is depicted in Fig. 5. The influence of the applied field E_a on the values of S_n is negligible.

It is worthy to note that $\Lambda < \Lambda_B$ gives $KL_D > 1$ in Eq. (8a), and hence $m_1 << m$. In this case $f(m_1) \approx h(m_1) = -m_1/2$, what means, that the Eq. (23) is satisfied for every value of m. On the other hand, if $\Lambda >> \Lambda_B$, the deviation from the linear function $h(m_1)$ takes place, however, it becomes significant for $m > 0.8$. The boundary grating period Λ_B is strongly dependent on the trap density. Larger trap density leads to shorter recombination times and diminish Λ_B (Fig. 6), in result the nonlinear behaviour appears for the smaller grating period.

The characteristic grating period Λ_B, was introduced in Ref. 27 as a quantity determining the PR grating resolution. This definition follows from the fact that substitution of Λ_B into linear solution of Eq. (10a) for the first harmonic gives approximately $\left|\tilde{E}_1\right| \approx (1/2)\left|\tilde{E}_1^{sat}\right|$, where $\tilde{E}_1^{sat}$ is the saturation value, appearing for $\Lambda \to \infty$. Thus, the grating is fully developed on the condition that $\Lambda > \Lambda_B$.

At last, according to Eq. (15), the value of the external field (in the linear transport regime) has a small influence on the nonlinearity of the space charge field and $\left|\tilde{E}_n\right| \sim E_a$ occurs with a good approximation.

7. Space charge field distribution

The spatial field distribution $E_{sc}(z)$ can be obtained from Eq. (14) or equivalently as a sum of the Fourier components

$$E_{sc}(z) \cong \sum_{n=1}^{N} \tilde{E}_n \cos(nKz + \varphi_n) \tag{25a}$$

$$\varphi_n = \arg(\tilde{E}_n) = \begin{pmatrix} -\pi \\ 0 \end{pmatrix}_{even}^{odd} + \arctan\left(\frac{\xi E_d}{E_a}\right) \tag{25b}$$

where phase shifts for even and odd components differ of a π.

The minimal number N of harmonics required to guarantee convergence of the space-charge field may be derived from the relationship

$$N_{\min}(m, \Lambda) = 1 - 1/\log\left|f(m_1)\right| \tag{26}$$

where we take only components fulfilling the criterion $|E_n|/|E_1| > 0.1$ [18]. The number N is a function of the mod-

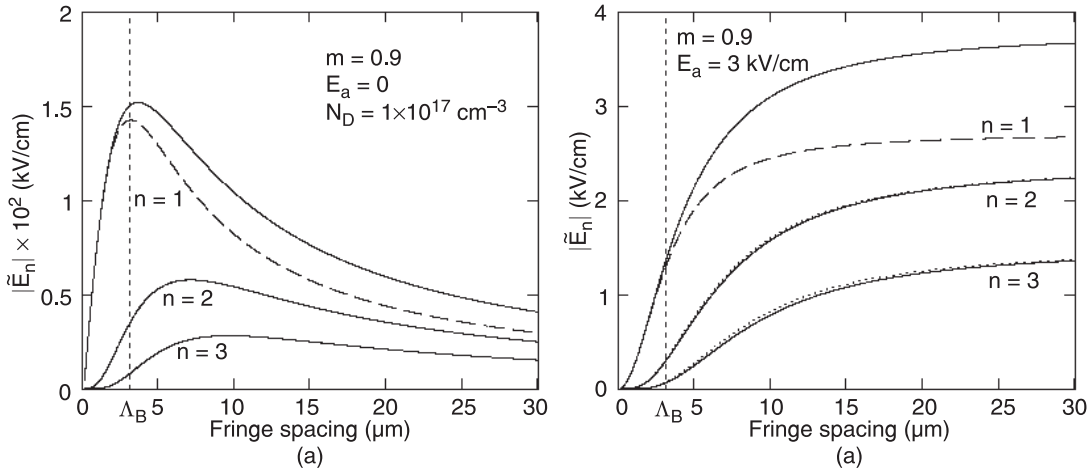

Fig. 4. The first three space charge field harmonics amplitudes as a function of the grating period: (a) without the applied electric field and (b) with an applied electric field; solid lines express numerical solutions of $f^n(m_1)E_n$, on the basis of Eq. (7), dotted lines express analytic solution Eq. (15a). The dashed line shows the linear solution of Eq. (10.1). The other parameters are in Table 1.

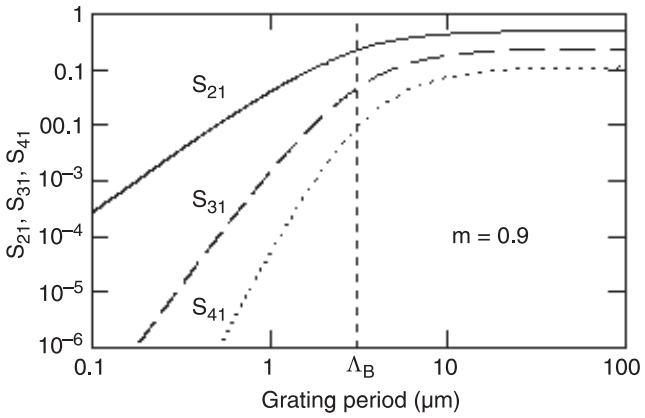

Fig. 5. The ratios of higher harmonic to the fundamental one versus the grating period obtained from Eq. (7). The characteristic period Λ_B = 3.1 μm. Other parameters identical like in Fig. 4.

ulation depth and the grating period, what is illustrated in Fig. 7. The number of harmonics increase rapidly for $m >$ 0.8 and for Λ larger than Λ_B. For the grating period much smaller then Λ_B, the first harmonic $N = 1$ is sufficient for arbitrary value of m. In Fig. 8, the $E_{sc}(z)$ and $N_D^+(z)$ profiles are shown for $\Lambda >> \Lambda_B$ and for three different values of m. The space-charge field reaches the maximum value $E_{sc}^{(\max)}$ in dark places ($z = (j + 1/2)\Lambda$, $j = 0,1,2...$), while the minimum value $E_{sc}^{(\min)}$ in bright ones ($z = j\Lambda$), screening the external field. If the diffusion is omitted, the extreme values obtained from Eq. (14) are

$$E_{sc}^{(\max)} = E_a\left(\sqrt{\frac{1+m_1}{1-m_1}} - 1\right), \qquad E_{sc}^{(\min)} = E_a\left(\sqrt{\frac{1-m_1}{1+m_1}} - 1\right). \tag{27}$$

The space-charge field obtained for $m > 0.8$ can be considerably higher then the external field. For the total electric field above 4 kV/cm the nonlinearity of electron transport which is not included in presented model should be taken into account. As it can be seen from Fig. 8(b) even for m =1 the depletion of the ionized donors concentration amounts to only several percents what confirm our earlier assumptions.

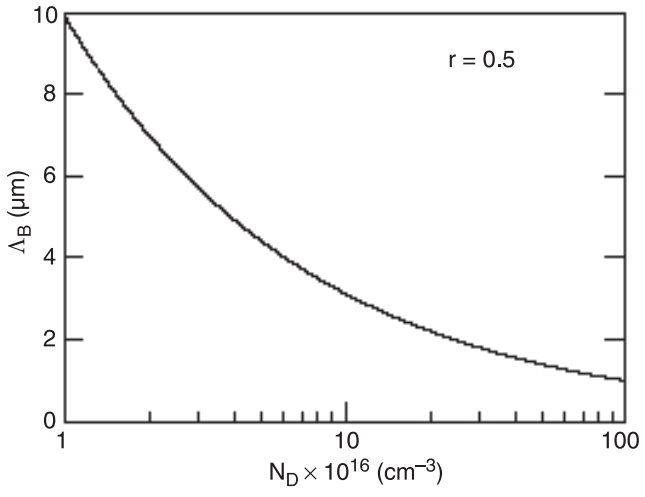

Fig. 6. The boundary grating period versus donors concentration for the constant donor compensation ratio.

8. Harmonics of photorefractive grating

8.1. Grating harmonics

For PR-MQW sample operating in the Franz–Keldysh geometry electrorefraction and electroabsorption approximately depend on square of the electric field. Changes in absorption and refraction may be written by means of the complex refractive index as [27,39]

$$\Delta\hat{n}(\lambda z) = -\frac{1}{2}n_f^3\hat{s}(\lambda)E_{tot}^2(z), \tag{28}$$

where $\Delta\hat{n} = \Delta n + i\Delta\kappa$, the extinction coefficient $\kappa = \alpha\lambda/(4\pi)$, n_f is the average refractive index of the material, $\hat{s} = s_1 + is_2$ is the quadratic electro-optic coefficient and $E_{tot} = E_a + E_{sc}$.

Harmonics components of the PR grating created by quadratic electro-optic effect are not proportional to the Fourier's components of the space charge field. In order to determine grating harmonics we substitute Eq. (21a) to Eq. (24) and after some algebra obtain the amplitudes

$$\Delta\tilde{n}_0 = -\frac{1}{2}n_f^3\tilde{s}\left(E_a^2 + \frac{1}{2}\sum_{\nu=1}^{N}\left|\tilde{E}_\nu\right|^2\right) \tag{29a}$$

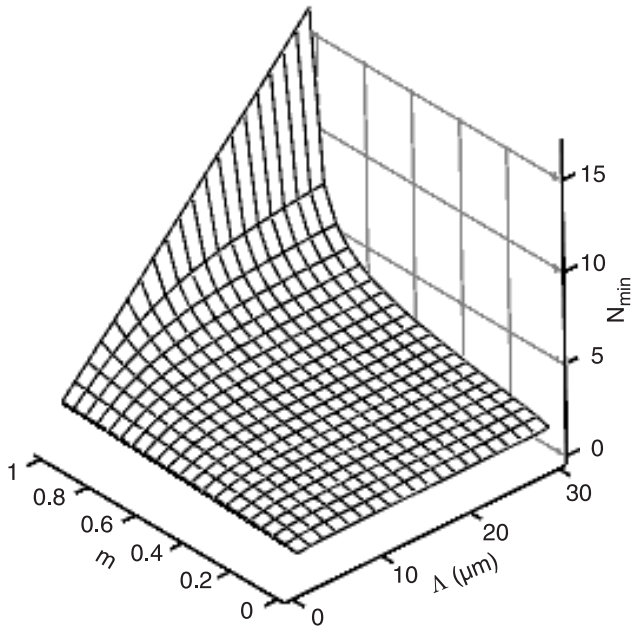

Fig. 7. Minimum number of harmonics required to the space-charge field convergence as a function of the modulation depth and grating period, for Λ_B = 3 μm.

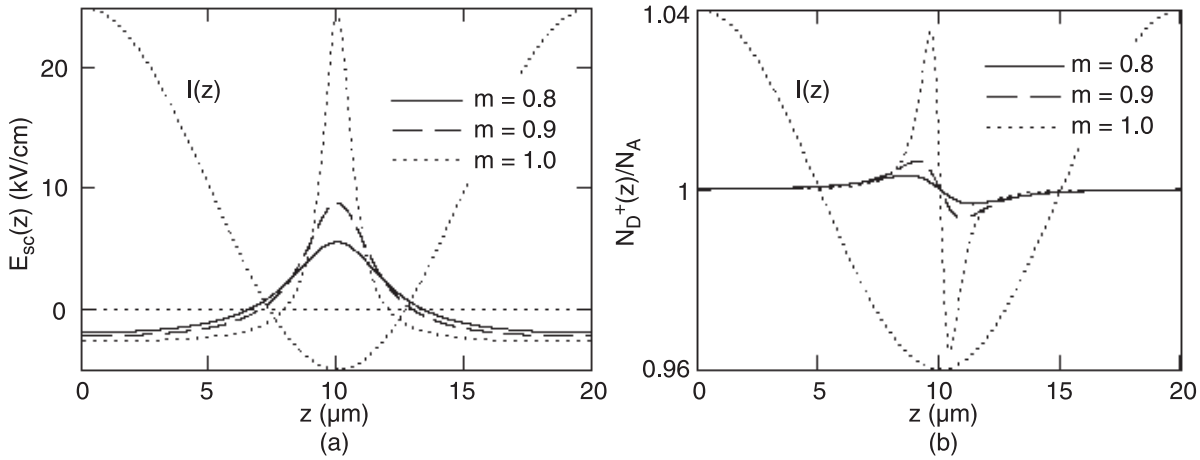

Fig. 8. The space charge field profile for different fringes contrasts (a) and the ionized donors density profile for the initial density $N_D^+(t=0) = N_A = 5\times10^{16}$ cm^{-3} (b). The results obtained for E_a =3 kV/cm, Λ = 20 μm, and Λ_B = 3 μm.

$$\Delta\tilde{n}_n = -\frac{1}{2}n_f^3\tilde{s} \times\left(2E_a\tilde{E}_n + \frac{1}{2}\sum_{\nu=1}^{n-1}\tilde{E}_\nu\tilde{E}_{n-\nu} + \sum_{\nu=1}^{N-n}\tilde{E}_\nu^*\tilde{E}_{\nu+n}\right) \quad (29b)$$

where $\tilde{E}_\nu$ are the amplitudes of the E_{sc} field according to Eq. (15a).

Optionally one can use directly the Fourier's transform formulas. In that case the space distribution for the refractive index is

$$\Delta n(z) = -\frac{1}{2}n_f^3 s_1 E_{tot}^2(z) = \Delta n_0 + \sum_n \mathrm{Re}(\Delta\hat{n}_n \exp(inKz)) \quad (30)$$

and distribution of the extinction coefficient, $\Delta\kappa(z)$, has an analogous form.

8.2. Dependence of the grating harmonics on basic parameters

Because the refractive index grating (RIG) and the absorption grating depend in the same manner on parameters variations, we reduce our analysis to RIG and use the space-charge amplitudes given by Eq. (15a). The electro-optic coefficients values, $s_1 = -4\times10^{-12}$ cm^2/V^2, electroabsorption close to zero $s_2 \approx 0$ and $n_f = 3.55$ used in the further calculations are taken from [27] for the wavelength λ = 835 nm, what corresponds to the localization of the heavy holes exciton peak in the described AlGaAs-GaAs MQW sample consisting of sixty periods of 7.5 nm GaAs and 10 nm $Al_{0.3}Ga_{0.7}As$. In the case of negligible diffusion, E_{sc} field components are proportional to the external field (sec. 6), therefore RIG harmonics are proportional to square of the external field $\Delta n_n \sim E_a^2$. This situation is shown in Fig. 9(a). In Fig. 9(b), the amplitudes Δn_n versus the grating period are plotted. Comparing this plot with $\tilde{E}_n(\Lambda)$ presented in Fig. 4(b) one can observe greater higher harmon-

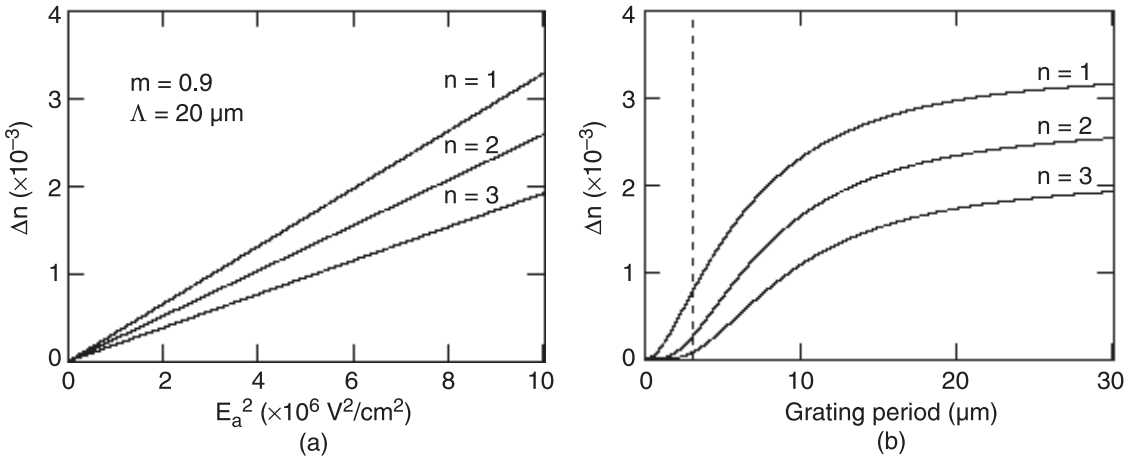

Fig. 9. Dependence of the refractive grating first three components on a square of the external electric field (a) and dependence of the components on the grating period, for the applied field of 3 kV/cm (b).

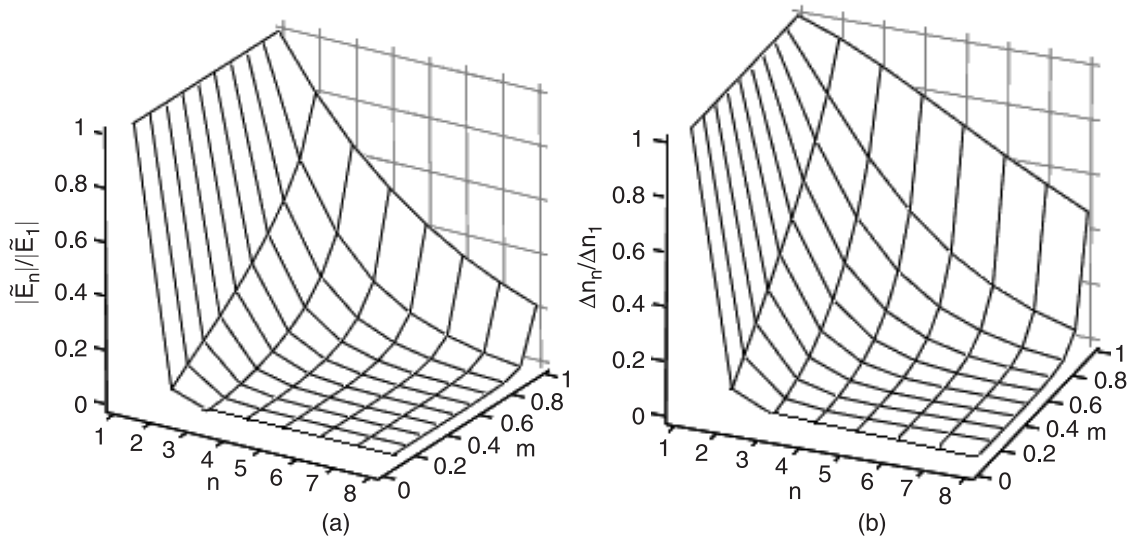

Fig. 10. Ratios of higher order amplitudes (n >1) to the first order one for (a) the space charge field and (b) the refractive index changes spectrum versus the light intensity modulation coefficient. Results obtained for $\Lambda = 20$ μm >> Λ_B and the applied field $E_a = 3$ kV/cm.

ics contribution. For the large grating periods ($\Lambda \to 0$) RIG amplitudes approach asymptotically the value

$$\Delta n_n^{\max} = -2n_f^3 s_1 E_a^2 f^n(m_1) \times \left(\frac{n+1}{2} + f^2(m_1) \frac{1 - f^{2(N-n)}(m_1)}{1 - f^2(m_1)} \right) \quad (31)$$

obtained from Eq. (29b) In particular it should be noticed, that the linear solution [$n = 1$ in Eq. (7)] with the neglected diffusion gives $\tilde{E}_1 = -mE_a$, what leads to the fundamental harmonics amplitude $\Delta n_1^{linear} = n_f^3 s_1 m E_a^2$. Whereas, when the higher harmonics contribution is taken into account, the refractive grating obtained from Eq. (31) with $n = 1$ and for the space charge field $\tilde{E}_1 = 2f(m)E_a$ takes the form

$$\Delta n_1^{\max} = \Delta n_1^{linear} 2f(m) \left(1 + f^2(m) \frac{1 - f^{2(N-n)}(m)}{1 - f^2(m)} \right). \quad (32)$$

For the small modulation depth $\Lambda n_1^{\max}$ tends to Δn_1^{linear}, however, for $m \sim 1$ the amplitude obtained from Eq. (32) can considerably exceed the value from the linear solution. By the reason of quadratic relation, the contribution of higher harmonics in the RIG spectrum is stronger than in the space-charge field amplitude spectrum. This behaviour is illustrated in Fig. 10, where the ratios of the higher order amplitudes (n >1) to the first order ones are for the space-charge field and for the refractive index changes, as functions of the fringe contrast are plotted.

Degree of nonlinearity for $E_{sc}(z)$ and $\Delta n(z)$ distribution depends simultaneously on m and Λ. Hence, in accordance with the conclusions from sec. 6 and Eq. (29b) one can find that for $\Lambda << \Lambda_B$ the relation $\Delta n_n \sim m^n$ is approximately fulfilled, whereas for $\Lambda > \Lambda_B$ the superlinear dependence versus m^n is predicted. The dependence of the first harmonic of Δn on Λ and m is illustrated in Fig. 11. The higher grating harmonics reveal similar behaviour.

In Fig. 12, the refractive index profile is plotted for the grating period of 20 μm >> Λ_B and for three different but this result is obtained under the assumption of the linear electrons transport. For the analysed PR-MQW one can expect the considerable influence of the nonlinear transport effect for $E_{tot} > 4$ kV/cm.

8.3. Diffraction efficiency

By the reason of strong absorption, PR-MQW devices are mostly used as thin holographic films (thickness of about 1–2 μm) working in the transmission geometry. Since usually the grating period is bigger then the film thickness ($\Lambda > L$), the conditions for the diffraction in the Raman-Nath regime are fulfilled and many orders of diffracted light appear. For complex n-th order harmonic grating ($\Delta n_n + i\Delta\kappa_n$)cos($nKz$), diffraction efficiency for the M-th order of diffraction is given by [27,35,39]

$$\eta_M \cong \frac{1}{2^{2M} M!^2} \left[\left(\frac{2\pi \Delta n_n L}{\lambda \cos\theta'} \right)^2 + \left(\frac{\Delta \alpha_n L}{2 \cos\theta'} \right)^2 \right]^M, \quad (33)$$

where θ' indicates the internal angle of the incident beam, and L is the sample thickness. In particular, for the strongest, first diffraction order (M = 1) Eq. (33) gives $\eta_1 \sim (\Delta n_n)^2, (\Delta \alpha_n)^2$. According to Fig. 11, for properly small grating periods ($\Lambda \le \Lambda_B$), $\eta_1(K) \sim m^2$, $\eta_1(2K) \sim m^4$, should be expected, where $\eta_1(K)$, $\eta_1(2K)$ are diffraction efficiency (M = 1) from the first and the second order spatial harmonic grating, respectively. This prediction stays in the agreement to experimental results [39]. However, for larger grating periods and the high fringes contrast, analysed model predict significant difference from $\eta_1^{(n)} \propto m^{2n}$. Unfortunately, we have not found any experimental data, that can confirm or not this prediction. Described relations are illustrated in Fig. 13.

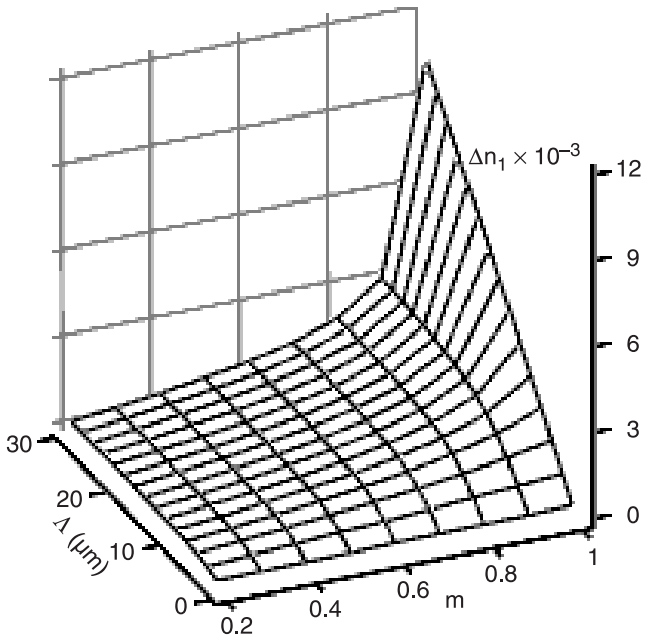

Fig. 11. Amplitude of the grating first harmonic as a function of the grating period and the fringes contrast. For small grating periods the relation $\Delta n_1 \sim m$ is correct in the whole range of m.

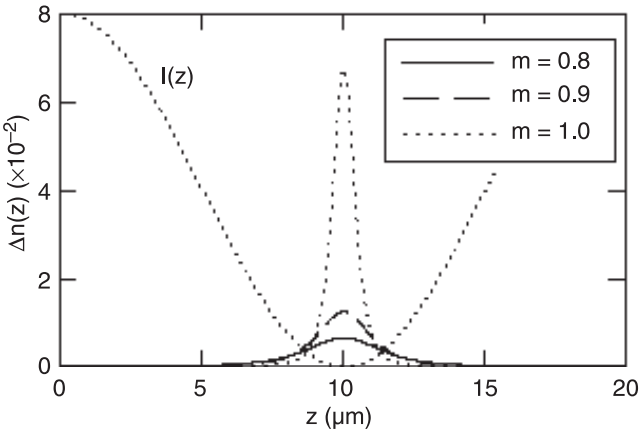

Fig. 12. Spatial distribution of the refractive index changes in the presence of external field of 3 kV/cm for different modulation depths of the interference pattern.

9. Conclusions

We found the analytic solution that describes steady-state space charge field induced in PR-MQW working in the Franz-Keldysh geometry by a high contrast interference pattern. Calculations were performed in frames of the PDDT model for electric field limited to linear transport regime. Moreover, it was found that the solutions for carriers densities obtained in frames of the perturbative approach (non-coupled equations) remain correct for arbitrary fringes contrast m. For high-enough effective traps concentration N_{eff} (i.e., in accordance with Fig. 2 for $N_{eff} >$ (5–10)×10^{15} cm^{-3}) free carriers distributions may be treated as quasi-sinusoidal. In this case, the modulation index m_1 of the free carriers grating can be derived from the linear solution for the fundamental harmonic. Application of this result to the classical PDDT model describing PR effect in bulk, nonresonant material enables us to improve the Moharam's solution by the replacement of the light modulation m with the carrier modulation m_1 being a function of Λ, E_a, and N_{eff}. Then, in the small contrast limit the Moharam's solution becomes equal to the classical Kukhtarev's solutions.

We found also that the characteristic period $\Lambda_B = 2\pi L_D$, (where L_D is the bipolar diffusion length) defining the resolution of PR-MQW elements, can be regarded as the boundary period separating the linear and nonlinear material response ranges. It makes a basic difference in comparison with the solution for conventional bulk materials, where the characteristic period is proportional to the Debye's screening length. It was shown that for the large modulation depths the quadratic electrorefraction enhances the contribution of higher harmonics in the refractive index spectrum in comparison with the space-charge field spectrum.

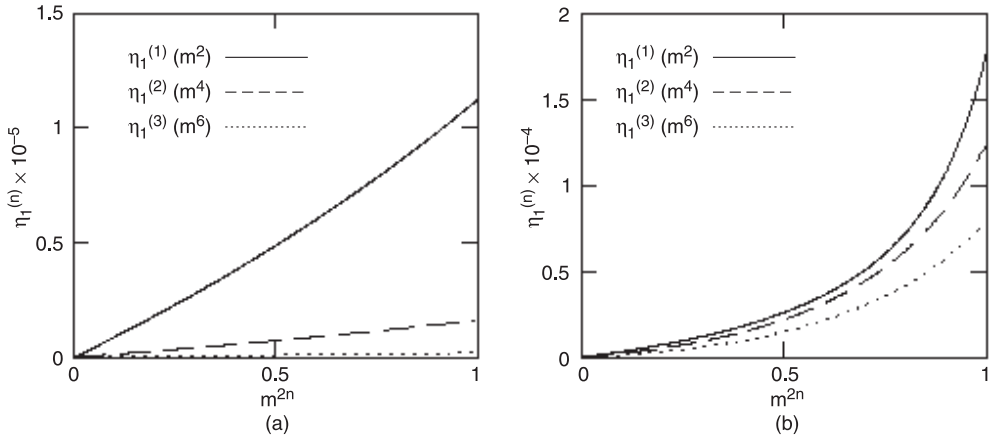

Fig. 13. Efficiency of the first order diffraction ($M = 1$) on the first three harmonics of the refractive index grating. In the case of two grating periods $\Lambda = 3$ μm ($< \Lambda_B$) (a) and $\Lambda = 10$ μm ($> \Lambda_B$) (b), as a functions of proper powers of the modulation depth m^{2n} ($n = 1,2,3$) for $\lambda = 835$ nm, $E_a = 3$ kV/cm.

Acknowledgments

This work was partially supported by the Polish Committee for Scientific Research (KBN) under the research project No. 3 T11B 076 26, performed in the years 2004–2006.

References

1. J.P. Huignard and P. Gunter, *Photorefractive Materials and their Applications II,* Springer-Verlag, Berlin, Heidelberg 1988.
2. P. Vaveliuk, B. Ruitz, N. Bolognini, and J. Fernandez, "Transient behaviour of the photorefractive space-charge field", *Phys. Rev.* B62, 4511 (2000).
3. N.V. Kukhtarev, V. Markov, S. Odulov, M. Soskin, and V. Vinetskii, "Holographic storage in electrooptic crystal. 1 Steady state", *Ferroelectrics* 22, 949 (1979).
4. G.C. Valley, "Two-wave mixing with an applied field and a moving grating," *J. Opt. Soc. Am.* B1, 868 (1984).
5. P. Yeh, *Introduction to Photorefractive Nonlinear Optics*, Wiley, New York, 1993.
6. M.P. Petrov, S.I. Stepanov, and A.N. Khomenko, *Photorefractive Crystals in Coherent Optical Systems*, Springer, New York, 1991.
7. G.A. Brost, "Photorefractive grating formation at large modulation with alternating electric fields", *J. Opt. Soc. Am.* **B9**, 1454 (1992).
8. E. Serrano, V. López, M. Carrascosa, and F. Agulló-López, "Steady-state photorefractive gratings in $LiNbO_3$ for strong light modulation depths", *IEEE J. Quantum. Electron.* **30**, 875 (1994).
9. A. Bledowski, J. Otten, and K.H. Ringhofer, "Photorefractive hologram writing with modulation 1", *Opt. Lett.* **16**, 672 (1991).
10. L.B. Au and L. Solymar, "Space-charge field in photorefractive materials at large modulation", *Opt. Lett.* **13**, 660 (1988).
11. P. Buchhave, "Computer simulation of multiple dynamic photorefractive gratings", J. *Opt. Soc. Am.* **B15**, 1865 (1998).
12. E. Serrano, V. López, M. Carrascosa, and F. Agulló-López, "Recording and erasure kinetics in photorefractive materials at large modulation depths", *J. Opt. Soc. Am.* **B11**, 670 (1994).
13. F. Vachss and L. Hesselink, "Nonlinear photorefractive response at high modulation depths", *J. Opt. Soc. Am.* **A5**, 690 (1988).
14. E. Serrano, M. Carrascosa, and F. Agulló-López, "Nonperturbative analytical solution for steady-state photorefractive recording", *Opt. Lett.* **20**, 1910 (1995).
15. E. Serrano, M. Carrascosa, and F. Agulló-López, "Analytical and numerical study of photorefractive kinetics at high modulation depths", *J. Opt. Soc. Am.* **B13**, 2587 (1996).
16. B.I. Sturman, F. Agulló-López, M. Carrascosa, and L. Solymar, "On macroscopic description of photorefractive phenomena", *Appl. Phys.* **B68**, 1013 (1999).
17. N.V. Kukhtarev, P. Buchhave, and S. Lyuksyutov, "Optical and electric properties of dynamic holographic gratings with arbitrary contrast", *Phys. Rev.* **A55**, 3133 (1997).
18. P. Vaveliuk, B. Ruiz, O. Martinez Matos, G.A. Torchia, and N. Bolognini, "An electron-hole transport model for the analysis of the photorefractive harmonic gratings", *IEEE J. Quantum Electron.* **37**, 1040 (2001).
19. P. Vaveliuk, B. Ruiz, and N. Bolognini, "Analysis of the steady-state photorefractive harmonic gratings", *Phys. Rev.* **B59**, 10985 (1999).
20. P. Vaveliuk, A. Lencina, P.C. de Oliveira, and N. Bolognini, "Photorefractive harmonic gratings within the shallow trap model", *IEEE J. Quantum Electron.* **38**, 1541 (2002).
21. R. Saxena and T.Y. Chang, "Perturbative analysis of higher-order photorefractive gratings", *J. Opt. Soc. Am.* **B9**, 1467 (1992).
22. S. Ducharme, J.C. Scott, R.J. Tweig, and W.E. Moerner, "Observation of the photorefractive effect in a polymer", *Phys. Rev. Lett.* **66**, 1846 (1991).
23. I.C. Khoo, "Holographic grating formation in dye- and fullerene C_{60}-doped nematic liquid-crystal film", *Opt. Lett.* **20**, 2137 (1995).
24. A. Partovi, "Photorefractive multiple quantum well materials and applications to signal processing", *Opt. Mat.* **4**, 330 (1995).
25. D.D. Nolte, D.H. Olson. G.E Doran, W.H. Knox, and A.M. Glass, "Resonant photorefractive effect in semi--insulating multiple quantum wells", *J. Opt. Soc. Am.* **B7**, 2217 (1990).
26. G. Montemezzani, P. Rogin, M. Zgonik, and P. Günter, "Interband photorefractive effects: Theory and experiments in $KNbO_3$", *Phys. Rev.* **B49**, 2484 (1994).
27. Q. Wang, R.M. Brubaker, D.D. Nolte, and M.R. Melloch, "Photorefractive quantum wells: transverse Franz-Keldysh geometry", *J. Opt. Soc. Am.* **B9**, 1626 (1992).
28. D.D. Nolte, "Semi-insulating semiconductor heterostructures: Optoelectronic properties and applications", *J. Appl. Phys.* **85**, 6259 (1999).
29. A Partovi, A.M. Glass, and D.H. Olson, "High-speed photodiffractive effect in semi-insulating CdZnTe/ZnTe multiple quantum wells", *Opt. Lett.* **17**, 655 (1992).
30. S. Iwamoto, H. Kageshima, and T. Yuasa, "Resonant photorefractive effect in InGaAs/GaAs multiple quantum wells", *Opt. Lett.* **16**, 321 (1999).
31. R.M. Brubaker, Q.N. Wang, D.D. Nolte, and M.R. Melloch, "Nonlocal photorefractive screening from hot electron velocity saturation in semiconductors", *Phys. Rev. Lett.* **77**, 4249 (1996).
32. D.D. Nolte, T. Cubel, and L.J. Pyrak-Nolte, "Adaptive beam combining and interferometry with photorefractive quantum wells", *J. Opt. Soc. Am.* **B2**, 195 (2001).
33. L.F. Magaa, F. Agull-Lpez, and M. Carrascosa, "Role of physical parameters on the performance of semiconductor multiple quantum well", *J. Opt. Soc. Am.* **B11**, 1651 (1994).
34. *Photorefractive Effects and Materials*, Chapt. 1, edited by D.D. Nolte, Kluwer, Dordrecht, 1995.
35. In Ref. 34, Chapt. 7.
36. In Ref. 34, Chapt. 1.
37. M.G. Moharam, T.K. Gaylord, and R. Magnusson, "Holographic grating formation in photorefractive crystals with arbitrary electron transport length", *J. Appl. Phys.* **50**, 5642 (1979).
38. E. Ochoa, F. Vachss, and L. Hasselink, "Higher-order analysis of the photorefractive effect for large modulation depths", *J. Opt. Soc. Am.* **B3**, 181 (1986).
39. Q.N. Wang, D.D. Nolte, and M.R. Melloch, "Spatial-harmonic gratings at high modulation depths in photorefractive quantum wells", *Opt. Lett.* **16**, 1944 (1991).

PRESS RELEASE

New 405nm Blue-Violet Laser Diode Modules with Modulated Output

Due to growing customer requirements, Photonic Products Ltd, the laser diode specialist, is adding 405nm (blue-violet) laser diode modules to its range of Photon Laser Modules. Designed as a complete laser diode system for OEMs, the 405nm laser modules are suitable for use in applications such as biomedical instrumentation, imaging, spectroscopy, fluorescence sensing, microscopy and many other emerging technologies.

The compact and efficient 405nm laser modules produce either an elliptical output beam of 4 x 1.5mm with output power of 4mW, or a 2mm circular output beam with output power of 0.9mW. The glass AR coated optical lens may be adjusted to produce either a collimated beam or focused spot. The standard lens may be replaced by other optical systems such as line generators.

The laser is extremely stable and reliable and offers the added advantage of TTL modulation input which will accept signals from DC up to 1 kHz minimum. TTL modulation can be used to enable, inhibit or modulate the laser.

Operating voltage is from 6.5V to 12V DC at an operating current of 90mA, or 100mA. Beam divergence is <0.6mrad for the circular output beam and <0.6 x 0.3mrad for the elliptical output beam. Operating temperature range is -10°C to +50°C.

The modules are cylindrical with an optional 25mm mounting flange and consist of an aluminium housing, laser diode, drive circuit and collimating lens. Mechanical dimensions are a compact 12 mm diameter x 43mm length. Electrical connections are made via external flying leads.

Photonic Products, established in 1995, is both a manufacturer of innovative optoelectronic components based on semiconductor laser diode technology and also a specialist distributor of high performance industrial laser diodes, LEDs and high performance optical lenses.

Data sheets are available to download from the Photonic Products website, http://www.photonic-products.com/products/laser_diode_modules/blue_modulation.html

